Promotion X2012
PROST Victor
En binôme avec
QUINTELA Julio

Ecole polytechnique - Massachusetts Institute of Technology

Rapport de Stage de Recherche
A brief insight into hydrodynamics

- Non Confidentiel -

Département : Mecanique
Champ: MEC593 Matière molle, fluides complexes, biomécanique et MEMES
Directeur de l'option : David Quéré
Directeur de stage: John Bush
Dates du stage: 01/04/2015 - 30/07/2015
Nom de l'organisme: Massachusetts Institute of Technology -Deparment of Mathematics
50 Ames Street, 02142 Cambridge, MA United States

Déclaration d'intégrité relative au plagiat

Je soussigné Prost Victor certifie sur l'honneur :

1. Que les résultats décrits dans ce rapport sont l'aboutissement de mon travail.
2. Que je suis l'auteur de ce rapport.
3. Que je n'ai pas utilisé des sources ou résultats tiers sans clairement les citer et les référencer selon les règles bibliographiques préconisées.

Je déclare que ce travail ne peut être suspecté de plagiat.

Date:

25 Juillet 2015

Signature:

Acknowledgment

First, I would like to thank David Quéré, who gave me the opportunity to do this internship.

Then, I want to warmly thank John Bush for his supervision, his brillant insights , ideas of projects and also for a fantastic week at HQA5 in Calabria.

I also gratefully acknowledge Dr. Dan Harris, P.-T. Brun and Adam Damiano for their precious help (experimentally and theoretically) and espacially thank Julio Quintela for being my partner on these projects.

Contents

1 Introduction **1**

2 Airflow Visualization of the Partial Coalescence of Soap Bubbles **2**
2.1 Introduction . . . 2
2.2 Experimental Setup . . . 2
2.3 Experimental Results . . . 3
2.4 Conclusion . . . 4

3 Visualization of Hydrodynamic Pilot-Wave Phenomena **5**
3.1 Introduction . . . 5
3.2 Experimental Setup . . . 5
3.3 Observations . . . 6
3.4 Conclusion . . . 7

4 Soap film dynamics leading to bubble pinch off **8**
4.1 Introduction . . . 8
4.2 Experimental Setup . . . 9
4.3 Experimental Results . . . 11
4.4 Theory of the vibrating membrane . . . 14
4.5 Wave velocity (Added Mass) . . . 14
4.6 Numerical simulations . . . 15
4.7 Pinch off criteria . . . 17
4.8 Mass redistribution - self adaptation . . . 19
4.9 Film thickness measurements . . . 19
4.10 Conclustion . . . 22

5 A hydrodynamic analog of the casimir effect **23**
5.1 Introduction . . . 23
5.2 Casimir effect . . . 23
5.3 Experimental study . . . 24
5.4 Theorical model . . . 26
5.5 Conclusion . . . 28

1 Introduction

This report prensents the work of four month's internship in John bush's froup at MIT Mathematics Department. I was paired with Julio Quintela Casal during this whole internship.

The goal of this internship was to conduct experimental and theoretical work on a multitude of projects. We both,extended som previous work and conducted from scratch some new projects. Each one of us worked on all the projects but we each focused on a particular one.

First, we extenteded the work of Dr. Daniel Harris on partial coalescing soap bubbles [18] and on the visualization of bouncing droplets [5].

Second, we conducted from the begining two projects, one on soap films and soap bubbles on which I was focused and one on a hydrodynamic analog of the casimir effect on which Julio was more focused.

This report is thus a collection of these four projects detailing the experiments, the results and the theoretical work.

2 Airflow Visualization of the Partial Coalescence of Soap Bubbles

2.1 Introduction

We here present the results of an experimental visualization of the airflow during the partial coalescence of soap bubbles. This study comes, as an extension of Pucci & Harris experimental work on the partial coalescence of soap bubbles [18]. When a soap bubble of radius R, surface tension σ is deposited on a horizontal soap film, it can undergo a partial coalescence as for a drop of water on a bath of water. The partial coalescence starts when the intervening air layer separating the film and the bubble has drained to a critical thickness. If the film ruptures at the point of contact, the high presssure air inside the bubble can be evacuated. At the same moment, the total collapse of the bubble is resisted by capillary waves that sweep up the bubble leading to the pinch-off of a smaller daughter bubble. This process can be repeated successively, giving rise to a coalescence cascade. The smoke inside the soap bubble enables us to see the airflow due to the overpressure in the bubble. The ejected air give rise to the formation of vortex ring of smoke because the ejected air is moving in a overall still air environment [21].

2.2 Experimental Setup

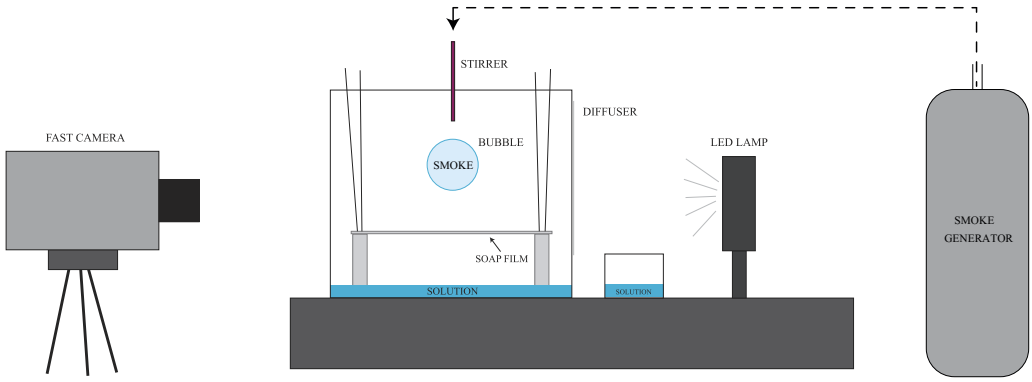

Figure 1: Schematic of the experimental setup.

The experimental setup is the same as Pucci & Harris setup, in which we added a smoke generator. It consists of a ceiled tank with a few access holes to move the $R_s = 6$cm acrylic circulare frame controlled by four wires attached at each corner of the frame. The ceiled tank creates a very humid environment, that reduces evaporation in the chamber and the influence of air currents, thereby extending the life of the soap film noticeably. The frame is dipped into the soap solution and placed vertically for a few minutes to allow it to thin by gravity in order to create a soap film of average thickness less than $h = 1\mu$m. A high-intensity lamp (Victor-Smith, 650 W) is placed on the side of the tank and a black background is placed behind the tank to visualize the smoke. A stirrer of inner diameter 2.5mm dipped into the soap solution and inserted through a small hole on the top of the tank is used to create the soap bubble with the smoke generator. A fast camera (Phantom V5.2 with a Nikon 105mm $f/2.8$ lens) placed in front of the tank acquires videos at 1000 frames/s (Fig.1). For this experiment, we used Pucci&Harris soap

mixture [18]. It is a solution of tap water and Dawn® Professional Detergent at 9.1% by weight. The concentration of the solution is well above the critical micelle concentration, which was estimated to be less than 0.1% and the surface tension is $\sigma = 24,3 \pm 2,2\text{mN/m}$.

2.3 Experimental Results

First of all, we tried to observe the partial coalescence studied by Pucci & Harris [18]. Cascades of until two partial coalescences were observed in our setup (Fig.2).

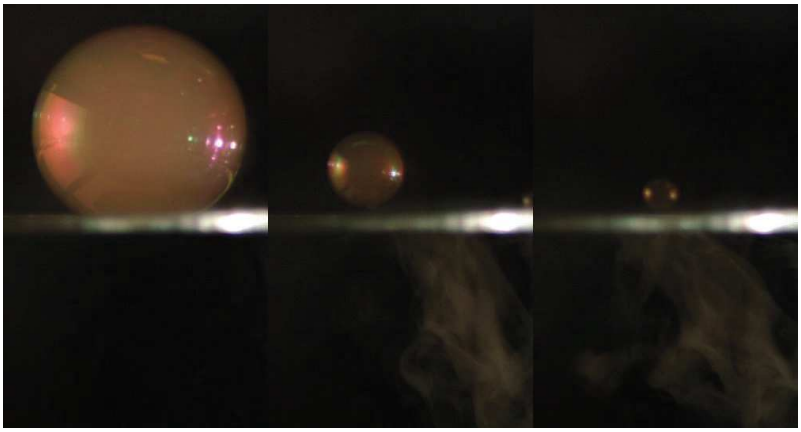

Figure 2: Timelapse of the coalescence cascade of a soap bubble on a soap film. The radius of each daughter bubble, is approximately half the radius of the initial bubble.

The airflow generated by the coalescing soap bubble was then recorded. The air in the bubble has an overpressure of $P_c = 4\sigma/R$ due to capillary pressure, with σ the surface tension and R the radius of the drop. When the coalescence is initiated and the soap film rupture underneath the bubble, the air is expelled by the capillary overpressure which is resisted by the inertia of the air being evacuated. Bernouilli's equation relates the overpressure initial velocity u of the air exiting the bubble:

$$\frac{4\sigma}{R} = \frac{1}{2}\rho_a u^2 \quad \text{so} \quad u = \sqrt{\frac{8\sigma}{\rho_a R}} \tag{1}$$

This compact volume of fast moving air in a stationary volume of air leads to the formation of a vortex [21] (Fig.3 & 4).

A second vortex ring can be observed after the pinch off of the daughter bubble. During the second pinch off, the soap film undergoes a very high surface deformation

Figure 3: Partial coalescing soap bubble with the ejected air forming a vortex ring.

singularity giving rise to a local increased curvature (see Fig.4 at $t = 23$ms). This high curvature leads to an ejection of a small compact mass of air at an important velocity (See Eq.1). This explains the small vortex ring passing through the first larger vortex ring as we can see on Fig.4 from time $t = 28$ms to $t = 42$ms.

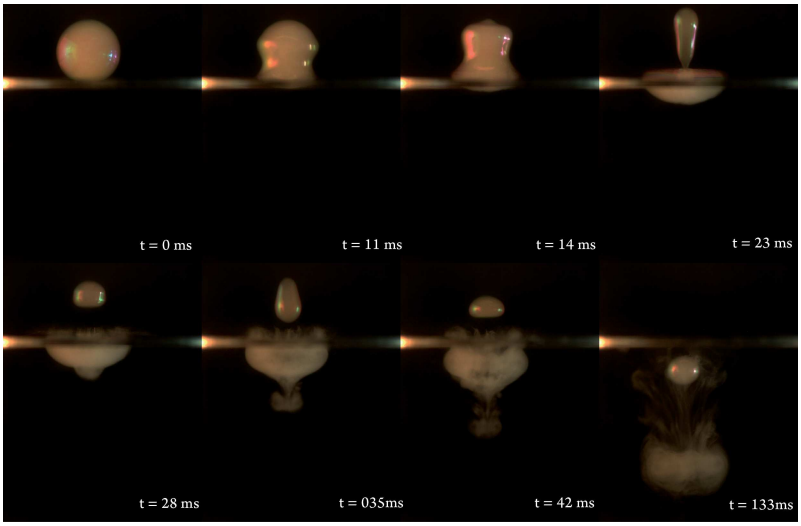

Figure 4: Timelapse of the coalescence of a soap bubble leading to the formation of a large and a small vortex ring. The radius of the initial soap bubble is $R = 5$cm

.

2.4 Conclusion

We have reported the first experimental visualization of the airflow during the partial coalescence of a soap bubble. The observations are in agreement with Pucci & Harris study [18]. The overpressure in the bubble ejects the air inside the bubble but not quickly enough to lead to a complete coalescence. Thus the initial air volume in the bubble is not entirely ejected and a smaller daughter bubble remains. In addition, the air ejection leads to the creation of one or two vortex rings at each coalescence process. The first one because of the overpressure in the initial bubble and a second one due to the overpressure from the critical curvature of the soap film during the pinch-off of the daugther bubble. A further study on the radius of the vortex ring regarding the soap bubble size and the curvature of the soap film could be conducted on the basis of this work.

3 Visualization of Hydrodynamic Pilot-Wave Phenomena

3.1 Introduction

Anyone who looks at the reflection of an object on water can appreciate the illusion of deformation created by undulations of the fluid surface. Painters and photographers have long exploited this mirroring effect, for example by reproducing reflected scenery distorted by ripples on a lake. We here exploit this phenomenon to visualize micrometric surface waves generated as a millimetric droplet repeatedly impacts a vibrating fluid bath [5]. This technics derives from D.Harris still photography technic used in his thesis. First, we briefly review the simple bouncing droplet apparatus used in the present work. Second, we report the optical method we used for simultaneously imaging the droplet and its waves by classical optical means despite the disparity in their size. Finally, we present some of the results obtained with this visualization technique.

3.2 Experimental Setup

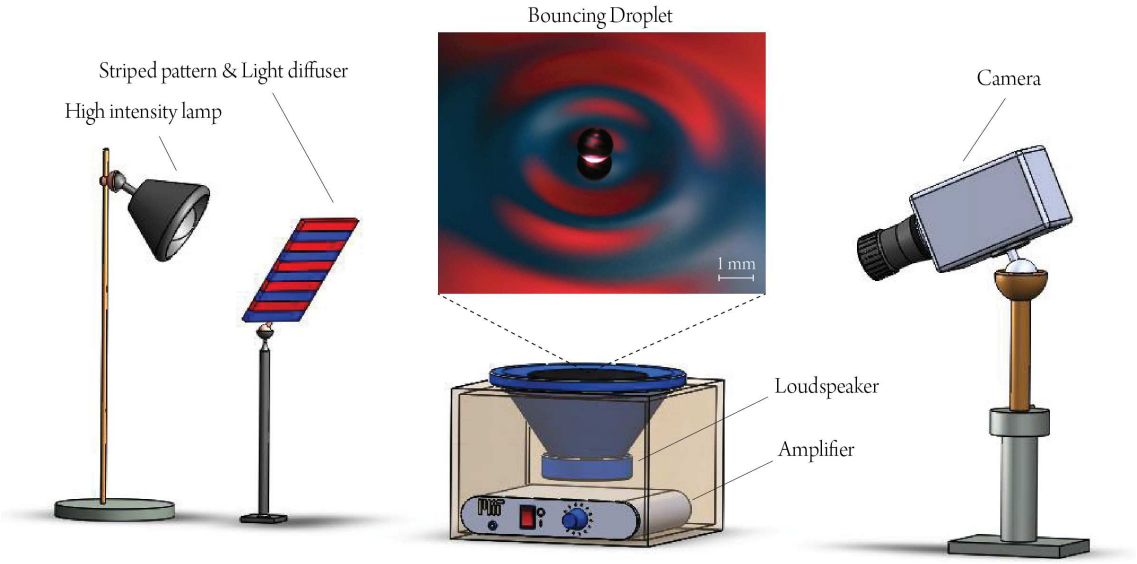

Figure 5: Schematic of the experimental setup.

The pilot-wave experiment (Fig. 5) was designed during the internship from D.Harris design [14] to provide a cheap demonstrator for educational purposes. The design explanation is available at the end of the report in the appendix. This setup consists of a 4" wide petri dish filled with 20 cSt Silicon oil (CAS 63148-62-9), driven by loud-speaker (Dayton Audio DC160-8 6-1/2"), which is connected to an amplifier (TMS 200W 12V) linked to a function generator (either by computer software or smartphone application). In a typical experiment, the forcing frequency is fixed ($f = 80$ Hz) and the amplitude A of the forcing is varied, thereby changing the peak acceleration $\gamma = A(2\pi f)^2$ of the bath. Above a critical acceleration amplitude γ_B, a droplet of the same fluid (generated by swiftly removing a needle from the bath) does not coalesce, but bounces indefinitely on the vibrating bath, exhibiting rich physical behavior [24]. For $\gamma > \gamma_w$, the bouncing state destabilizes, giving way to a walking state in which the drop propels itself across the surface by virtue of a resonant interaction with its own wave [8]. When γ exceeds a

critical value γ_F the free surface becomes unstable to a field of Faraday waves [13].The optical method developed here offers a visualization technique for all of these phenomena.

The lighting system consists of a high-intensity lamp (Victor-Smith 650 W) directed towards the bath. A transparent film with colored strip patterns is mounted to a frosted diffuser and placed between the lamp and the bath. We image the surface of the bath with a color high-speed camera (Phantom V5.2 with a Nikon 105mm $f/2.8$ lens and a Nikon 2X teleconverter) configured to 1000 frames per second and a $f/8$ aperture setting. The colored stripes reflect on the bath surface, and the camera is focused on the bouncing droplet. The base of the dish is painted black in order to minimize the reflections from the base of the container. A typical observation is reported in Fig.5. The size of the striped pattern was selected so that the periodicity of the reflected pattern approximately matches the wavelength of the waves generated by the droplet. Thus we can accurately visualize the interactions between the droplet and the underlying bath, several examples of which are depicted in Fig.6 (Supplementary Materials are available for more videos and images).

3.3 Observations

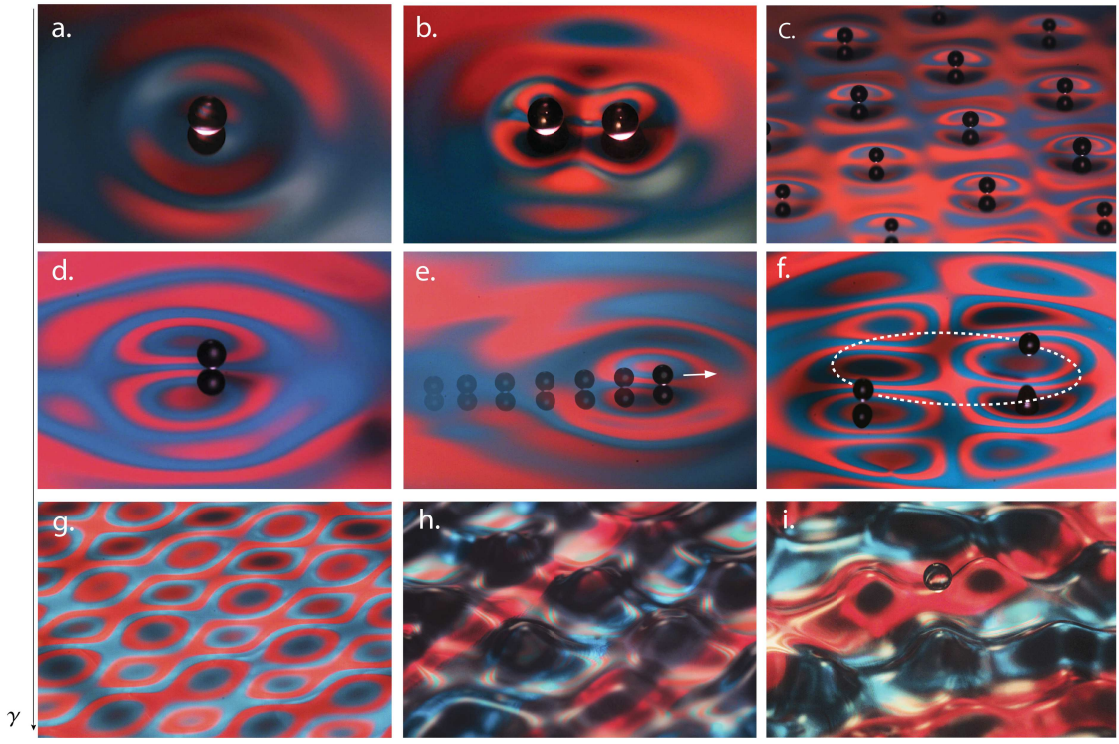

Figure 6: Different phenomena observed as the driving amplitude of the bath is increased (a) Bouncing droplet. (b) Bouncing pair (c) Droplets bouncing in a stable lattice. (d) Walker (e) Timelapse of a video of a walking droplet. The arrow points the direction of the droplet's horizontal motion. (f) Orbiting pair of droplets. The dotted line indicate the counter-clockwise motion of the drops. (g) & (h) Faraday waves. (i) Droplet created by Faraday waves. Droplets are of approximately 1mm diameter. (movies of the same views are supplemented in the oral presentation slides.)

If multiple bouncing droplets are positioned near one another, they may lock into

stable geometrical patterns [12] forming bouncing pairs or lattices as reported in Fig.6b,c. When the acceleration of the bath is increased a droplet may begin to walk, piloted by its own wave field [5] (Fig.6d,e).Two walking droplets directed towards each other can spontaneously orbit around one another [17](Fig.6f).

Above the Faraday threshold, surface deformations are much larger than those generated by the bouncing droplets and thus the light provided by the lamp is not reflected directly into the camera, resulting in dark images. This difficulty may be partially resolved by placing a mirror with the horizontal striped pattern on the bottom of the petri dish, which assists in revealing the phenomenon by reflecting the light towards the camera and unveiling the Faraday waves. (Fig.6e,h). At even higher accelerations the interface can break [22], forming multiple droplets which bounce chaotically on the Faraday waves(Fig.6i).

A strobe effect can be obtained by setting the frame rate of the camera to the bouncing frequency of the droplet. In our case, when the bath is forced at 80Hz the bouncing frequency is exactly 40Hz [5]. A single image of the droplet is captured at each period. This way the vertical dynamics of the droplet is filtered out, so that the droplet appears to hover over the surface. Setting the phase of the forcing or the camera, allows us to control the apparent vertical position of the droplet. Fig.6e was obtained through this technique.

3.4 Conclusion

We have reported the first experimental visualization of surface waves and bouncing droplets through deformed pattern reflection. The observations are in agreement with studies on the pilot wave phenomena. We were able to vizualise, surface waves generated by walkers, orbitals, boucing lattices, and Faraday waves. Through this work, we uncovered some phenomena such as instabilities in orbitals due to differences in dropsizes, constraining walkers to linear and circular corrals to control their positions to capture their dynamics with the camera and the merging of orbiting droplets in an unstable tight orbit. This technique could be further used with different capturing frames rates from the camera such as a slightly detuned frequency to capture a slowly bouncing droplet on a large time scale.

4 Soap film dynamics leading to bubble pinch off

Abstract

A strongly non-linear behavior of a soap film undergoing large-amplitude harmonic oscillations in the low frequency range is presented in this work. In such a film, liquid is re-distributed towards its center and the large-amplitude modes lead to the ejection of bubbles of the size of the main wave length from the film. Both processes, liquid re-distribution and bubble ejection, finally result in the rupture of the film.

4.1 Introduction

Soap films have fascinated people for a long time with their iridescent colors under the sun, and their ability to form bubbles that marvel the audience. This fragile and fleeting beauty is still after many decades a matter of many research work. Soap films are elastic membranes consisting of a nanometric to micrometric thick liquid film stabilized by surfactants. Soap films are mainly under control of surface tension aiming at minimizing its surface energy. This characteristic of soap films leads to striking geometrical shapes representing minimal surfaces such as spherical bubbles, helicoids or the well known catenoid. Saop films have also been largely studied as being an impressively accurate model for vibrating membranes [7].The tension is due to surface tension and the Marengoni elasticity that arises from the surfactant dynamics [4]. However, in a soap film, the inertia of the air moving around the film is no longer negligble and has to be accounted for as the inertia of the liquid film [7].

The basic behavior of a vibrating soap film is similar to that of standard elastic membranes, but in the soap film dynamics, there are mass redistributions and surfactants effects that lead to a broad range of new phenomena. In the case of small amplitudes and very thin films, counter-rotating vortices appear, showing evidence of rapid recirculation [1,23]. On the contrary, with thicker films and at higher amplitudes, liquid is redistributed permanently from the nodes to the antinodes. The system thus retains large amplitude oscillations at all frequencies. This effect called "self-adaptation" [2], leads to new mode formation and instabilities such as droplet ejection from the antinode [11].

Previous studies have mainly focused their interest at small amplitude oscillations. We here present an investigation of the soap film response to high amplitude forcing where strong non-linear behaviours arise leading to the formation of new modes, droplets ejection, instabilities (bubble creation through a pinch off of the interface) and finally to the rupture of the film.

A horizontal square soap film of density ρ, viscous damping β, surface tension σ and wave velocity c is forced into vibration through the high amplitude oscillations of the frame. The dynamics of the film are recorded through a high speed camera. Representative views of the film response are displayed in Fig.7. After a fast transient regime $\tau_t \sim 2/\beta c \sim 0,2$s, the soap film vibrates at the same frequency as the forcing but phase-shifted. The soap film then displays increasing deformations and oscillations through self-adaptation. Above an amplitude threshold, the deformations of the soap film lead to the creation of a soap bubble of approximately the size of half the wave length through the pinch off of the interface. Both mechanisms, liquid redistribution and bubble creation, finally lead to the rupture of the film. This present work focuses on the interface pinching off into soap bubbles.

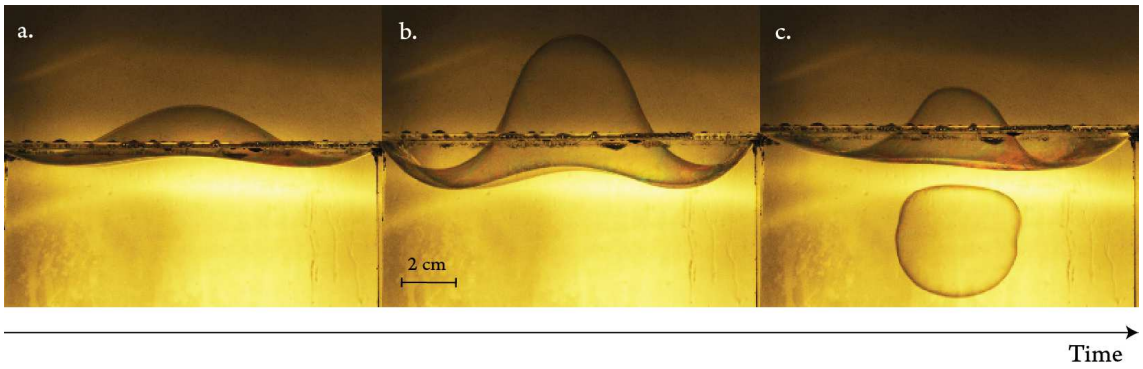

Figure 7: Overall film behaviour with time at constant frequency $f = 15$Hz and amplitude $A = 5$mm. During the transient response, oscillations and deformations are small (a). Then after mass redistribution, large-amplitude oscillations and deformation are observed (b), leading to the creation of a bubble (c).

4.2 Experimental Setup

The experimental setup consist of a $L = 12.7$cm acrylic square frame clamped on a shaker. A squeegee is dipped into the soap solution and then applied on the frame from one edge to the other in order to create a soap film of average thickness $e = 2\mu$m (see Sect.4.9.2). The frequency f is set to a fixed value between 3 to 30Hz during the experiment. A high-intensity lamp (Victor-Smith, 650 W) is placed behind the shaker and light is diffused by a translucent sheet. A fast camera (Phantom V5.2 with a Nikon 105mm $f/2.8$ lens) placed in front of the box acquires videos at 800 frames/s (Fig.8). For the present experiment, we used Pucci&Harris soap mixture [18]. It is a solution of tap water and Dawn® Professional Detergent at 9.1% by weight. The concentration of the solution is well above the critical micelle concentration, which was estimated to be less than 0.1% and the surface tension is $\sigma = 24,3 \pm 2,2$mN/m.

Under mechanical forcing, the soap film undergoes the highly reproducible sequence of events as shown in Fig.7 and explained in the Introduction (Sect.4.1).

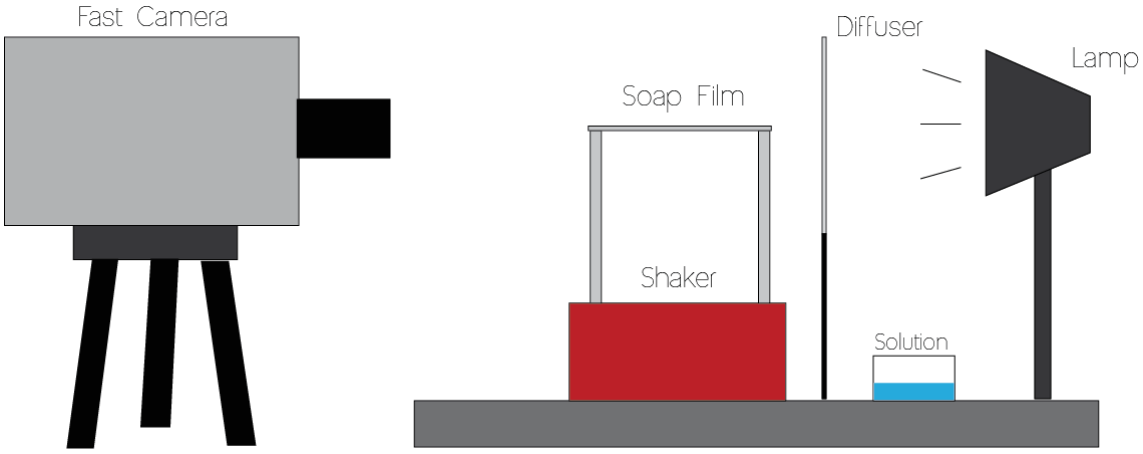

Figure 8: Schematic of the experimental setup.

Several shakers were used for the experiment. The frame was in a first place mounted on a loudspeaker (Dayton Audio DC300-8 12"). With this system it is not possible to set independantly the amplitude and the frequency of the forcing . After establishing a frequency sweep at a fixed intensity with an accelerometer (Arduino accelerometer Kootek GY-521 MPU-6050) it was noticed that there is a resonance around 11Hz and then the amplitude decreases with the frequency (see Fig.9). This system was used to verify the bubble pinch off phenomenon and to find the viscous damping parameter in the numerical model (see Sect.4.6). With the loudspeaker we can only trigger the bubble pinch off in a narrow range of frequencies (10 to 11Hz). The loudspeaker provides a wide range of frequencies but does not have a linear response in the range of frequencies we are interested in (3 to 30Hz). By working with a smaller frame, the same phenomenon can be exhibited under higher forcing frequencies (see Sect.4.4) but in that case, the amplitude of the forcing from the loudspeaker is too low to have the bubble pinch off from the soap film.

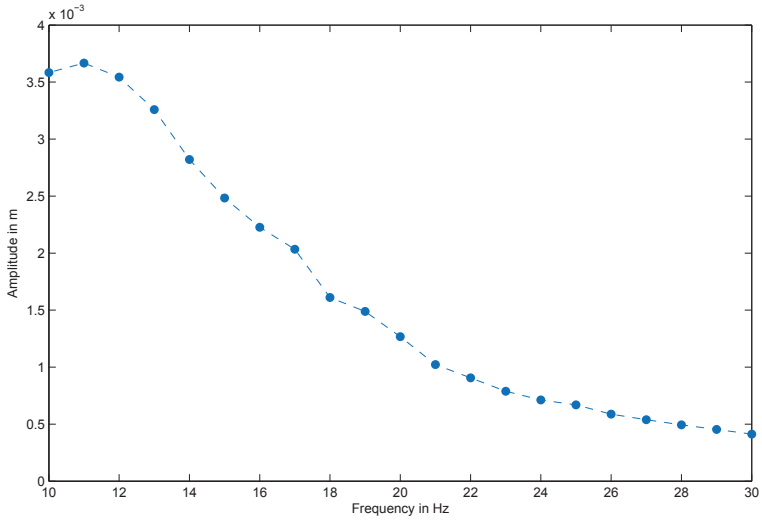

Figure 9: Amplitude of the loudspeaker oscillation at a fixed intensity during a frequency sweep. The amplitude was recorded through an accelerometer with less than 1% error.

From a permanent magnet DC motor (Dayton 4Z380A) we built a crank shaft system to provide the vertical forcing (see Fig.10). For this shaker, the forcing frequency range is 3 to 16Hz and the amplitude range is 5 to 15mm. This system allows us to set independently the amplitude and the frequency of the forcing on the soap film. Moreover it provides a sufficently high forcing amplitude to give rise to the bubble pinch off in the soap film almost in the entire forcing frequency range. This second shaker was used to conduct many of our experiments. This system is not ideal because it does not enable us to change continuously the amplitude of the forcing. A discrete number of forcing amplitude is available to us and we need to dismantle the setup each time we need to change the forcing amplitude. Moreover, this shaker is limited to $f = 16$Hz whereas the bubble pinch off phenomenon can be exhibited for higher frequencies.

Both this mechanical shaker and the loudspeaker have their flaws but they are a compromise between a high end shaker and a very cheap shaker.

Figure 10: Image of the crank shaft system setup, with ajustable crankpins to set different forcing amplitudes. The square frame of the soap film is mounted on vertical rail guides actuated by the connecting rod.

4.3 Experimental Results

In this section the experimental results with the loudspeaker and the mechanical shaker are presented. The main features of the soap film dynamics are the maximum amplitude A_s of the soap film oscillations and the main wave length (mode) λ_{mn} of the film response to forcing. These are the two parameters that contribute to the bubble pinch off (see Sect.4.7) and that are recorded during our experiments.

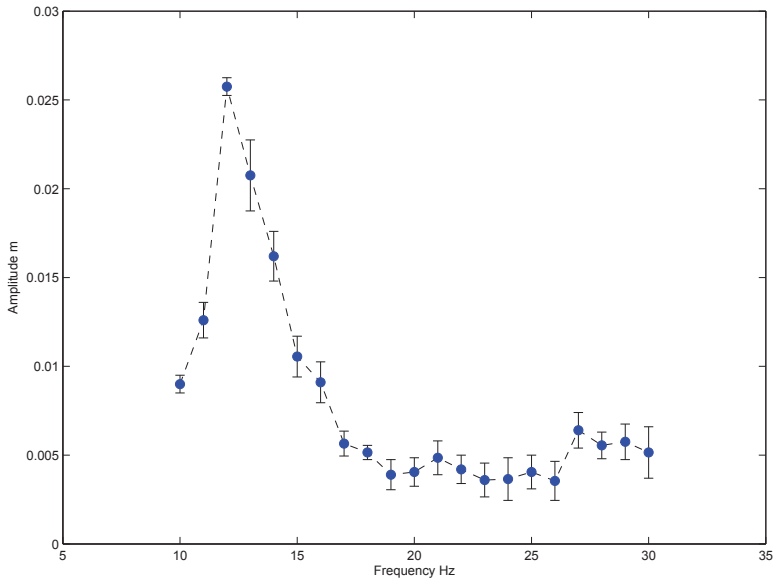

Figure 11: Maximum amplitude A_s of the soap film oscillations on the $L = 12,7$cm frame when forced with the loudspeaker

In the first place, the response of the soap film to the forcing was recorded by retreiving the maximum amplitude of the soap film oscillations A_s. The soap film presents some resonance when the forcing frequency excites a mode of the soap film. With the loudspeaker, the amplitude of the forcing varied with the frequency so we could not work at a fixed amplitude when performing the frequency sweep. In that case, only one of

the resonances is visible in the experimental data, around $f = 12$Hz (Fig.11). However, through the analytical study, it was noticed that the max amplitude A_s of the soap film at a fixed frequency, varied linearly with the forcing amplitude (see Sect.4.4). This characteristic allowed us to analyse the data obtained with the loudspeaker by multiplying the max amplitude A_s accordingly so that it appears like the soap film was under a fixed forcing amplitude. We were thus able to make a correspondance between the data from the loudspeaker and the one from the mechanical shaker. The following data on Fig.12 presents the maximum amplitude A_s of the soap film oscillations at a fixed forcing amplitude $A = 0.05$m when the forcing frequency varies from 3 to 30Hz on a square frame of size $L = 0.127$m. In this data, we can notice the soap film resonance at mode (1,1) with $f_{(1,1)} \simeq 4$Hz, mode (1,3)+(3,1) with $f_{(3,1)+(1,3)} \simeq 13$Hz, mode (5,1)+(1,5) with $f_{(5,1)+(1,5)} \simeq 29$Hz.

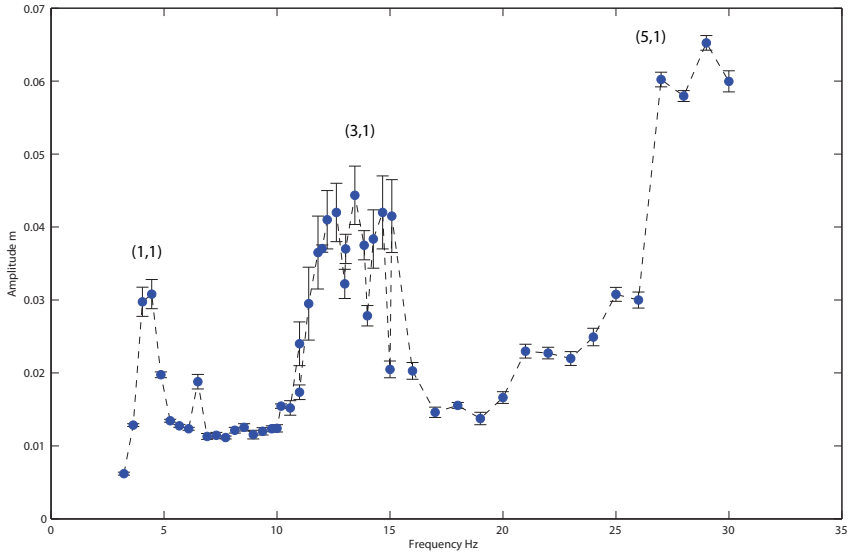

Figure 12: Maximum amplitude A_s of the soap film oscillations on the $L = 12,7$cm frame when forced by both the loudspeaker data and mechanical shaker data

When the oscillations of the soap film become large enough, they break, leading to the pinch off of soap bubbles Fig.13-14. At each forcing frequency, a critical forcing amplitude can be found, A_c, above which bubbles are ejected from the soap film (see Sect.4.7). The bubble ejection starts with very few bubbles ejected and with an important time between each ejection. This time corresponds to time during which liquid is redistributed in the film, since the ejection of the bubble creates a new mass distribution within the film. Then the ejection rate increases with forcing amplitude. Since the bubbles are ejected by breaking the surface wave, their diameter is expected to scale as $d_b \sim \lambda$. When the bubble pinch off occures, it was noticed that the diameter of the bubbles were of the scale of the wave length but, for the same wave length, when the driving was higher the diameter of the bubbles were larger. This could be due to the fact that with higher driving, the inertia is bigger and it streches more the soap film before the pinch off, leading to a larger bubble. The pinch off of the bubble was then reported into Fig.15. After crossing a threshold of amplitude and frequency, we obtain bubble pinch off when the soap film oscillates. After several bubble pinch off, the soap film becomes very thin and rapidly breaks (the soap film last around 1 min due to the thinning and evaporation).

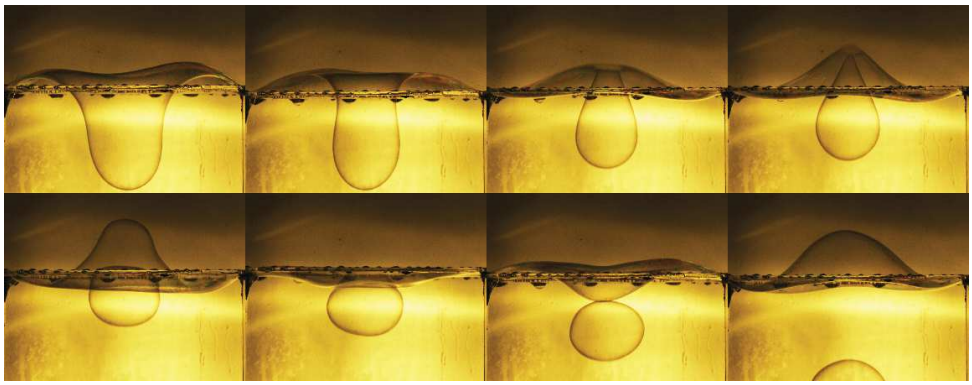

Figure 13: Breaking of the interface leading to bubble creation at $f = 12,6$Hz on a frame of $L = 12,7$cm

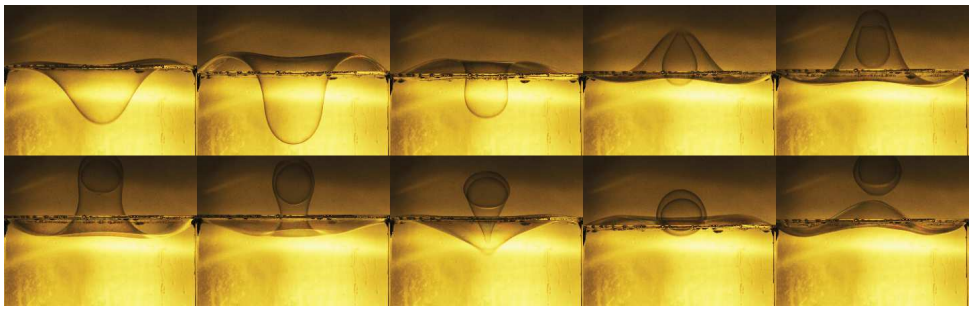

Figure 14: Breaking of the interface leading to the formation of a double bubble $f = 11,8$Hz on a frame of $L = 12,7$cm

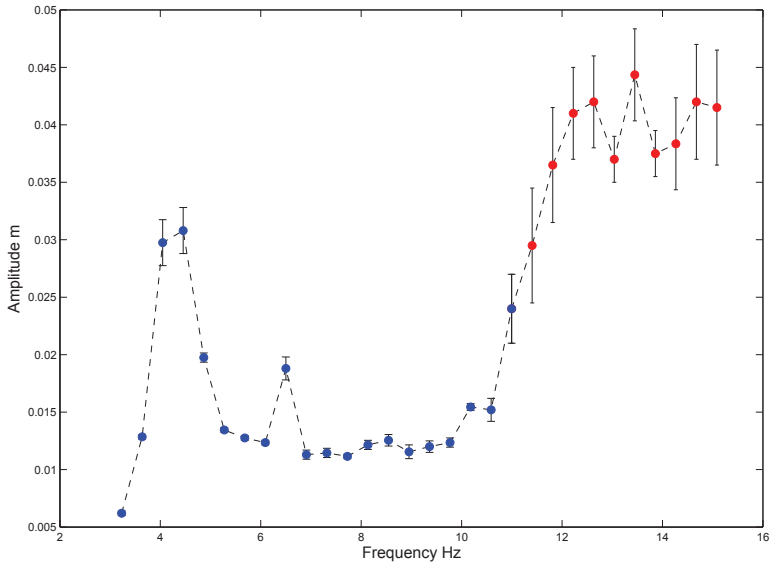

Figure 15: Amplitude of the soap film oscillations on the $L = 12,7$cm frame, with the mechanical shaker. The blue points correspond to a soap film response that did not lead to a bubble pinch off. The red points are soap films where bubble pinch off occured. The maximum amplitude is in that case, the mean maximum amplitude between two bubble pinch off.

4.4 Theory of the vibrating membrane

To have a qualitative idea of the dynamics of the soap film, we studied the forced vibration of a damped membrane [20]. The membrane is studied in the linear case (small amplitude vibrations) when forced by the oscillating clamped boundaries. The equation depicting the membrane is the following one:

$$\frac{\partial^2 z}{\partial t^2} + \beta c \frac{\partial z}{\partial t} - c^2 \Delta z = 0 \tag{2}$$

$$z = A\cos(\Omega t) \quad \text{on} \quad \partial\Omega \tag{3}$$

To resolve this equation, we place ourselves in the framework of the oscillating boundaries, $z = \bar{z} + A\cos(\Omega t)$. By writing that $\bar{z}(x, y, t) = f(x)g(y)h(t)$, the analytical solution of this equation is given by:

$$\bar{z} = \sum_{i=0}\sum_{j=0} Z_{2i+1,2j+1} \tag{4}$$

$$Z_{mn} = \frac{16A\Omega}{mn\pi^2} \frac{\sqrt{\Omega^2(\omega_{mn}^2 - \Omega^2 - \beta^2c^2)^2 + \beta^2c^2\omega_{mn}^4}}{(\omega_{mn}^2 - \Omega^2)^2 + \beta^2c^2\Omega^2} \sin\left(\frac{n\pi x}{L}\right) \sin\left(\frac{m\pi y}{L}\right) \cos(\Omega t + \Phi_{mn}) \tag{5}$$

$$\omega_{mn} = \frac{c\pi}{L}\sqrt{n^2 + m^2} \tag{6}$$

$$\Phi_{mn} = \cot^{-1}\left(\frac{\Omega(\omega_{mn}^2 - \Omega^2 - \beta^2c^2)}{\beta c \omega_{mn}}\right) \tag{7}$$

The solution provided us with the following information. The membrane is oscillating at the same frequency as the forcing with a phase shift. The forcing amplitude is linear with the membrane vibration amplitude Eq.(5). With this system, only the odd modes are excited Eq.(4). If we want to have a precise mode we can find it using the dispersion relation Eq.(6). Also, the dispersion relation show us that to observe the same mode on a half-size frame and soap film, we have to double the forcing frequency. This analysis of the linear case provides us with a strong insight of the soap film dynamics in the non-linear case.

4.5 Wave velocity (Added Mass)

The basic wave velocity of a vibrating membrane of thickness e and tension 2σ is:

$$c = \sqrt{\frac{2\sigma}{\rho e}} \tag{8}$$

In our case, the surrounding air plays a crucial role in the dynamics of the soap film. It acts as an added mass on the soap film, thus changing the wave velocity relation. A first approximation of the wave velocity with added mass, considers a constant added mass only function of the size of the membrane. It was computed by Minanmi [16] in the following form:

$$c = \sqrt{\frac{2\sigma}{\rho e + 0.68\rho_{air} L}} \tag{9}$$

A second approximation made by Couder & al [7] considers a varying added mass linearly proportional to the wave length of the soap film oscillations :

$$c = \sqrt{\frac{2\sigma}{\rho e + \rho_{air}\lambda}} \tag{10}$$

For our model, we mainly took into account the first approximation of the wave velocity with added mass.

4.6 Numerical simulations

In this section, the numerical simulations of the soap film as a vibrating membrane with a tension σ are presented. This model does not take into account the mass redistribution but takes into account the first approximation of the added mass. The equations are written in the frame of the oscillating frame:

$$\frac{\partial^2 z}{\partial t^2} + \beta c \frac{\partial z}{\partial t} - c^2 \Delta z = A\Omega^2 \cos(\Omega t) - A\Omega \sin(\Omega t) \tag{11}$$

$$z = 0 \quad \text{on} \quad \partial\Omega \tag{12}$$

$$c = \sqrt{\frac{2\sigma}{\rho e + 0.68\rho_{air} L}} \tag{13}$$

A finite difference method, with a centered scheme in space and time was used to run the simulations. Thus, a CFL condition (Eq.14) was required to make the simulation converge.

$$\delta t < \frac{1}{2c} \min(\delta x, \delta y) \sqrt{\frac{\beta^2 \min(\delta x, \delta y)^2}{16} + 2} - \frac{\beta \min(\delta x, \delta y)^2}{8c} \tag{14}$$

The viscous damping parameter β of the soap film was retrieved by fitting with a least square methods the numerical simulations to the experiments of the vibrating soap film on the loudspeaker. Through a frequency sweep in the experiments and in the numerical simulations, the maximum ampltitude of the soap film was recorded (Fig.11 experimental results) after a time $\tau_t \sim 2/\beta c \sim 0,2\text{s}$ (knowing that $\beta \sim 10\text{m}^{-1}$ by a qualitative look on the numerics compared to the experiment) that corresponds to the transient regime of the soap film response. The two curves were fitted to find the viscous damping in the soap film, $\beta = 13\text{m}^{-1}$. The louspeaker was used eventhough the amplitude varied with the frequency, which was accounted for in the numerical simulation, because it allowed a bigger range of frequencies and lower amplitudes so the redistribution of the mass in the film that was not accounted for in the numerical model is not too present.

Through the numerical simulations we could then retreive the qualitative response of the soap film through a forcing at a given frequency and amplitude Fig.16–18.

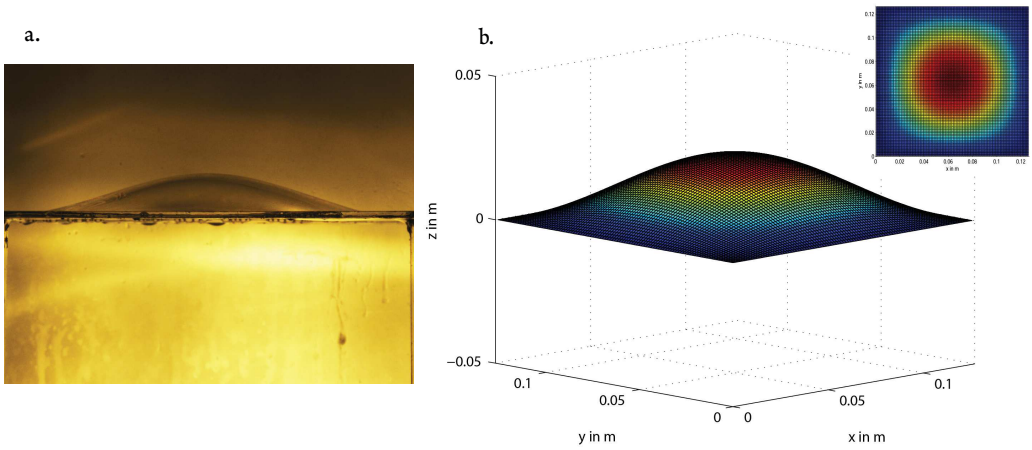

Figure 16: Visualization of mode $(1, 1)$ with the numerical model, at a forcing amplitude of $A = 0.005$m (b) and the corresponding visualization in the experiment (a)

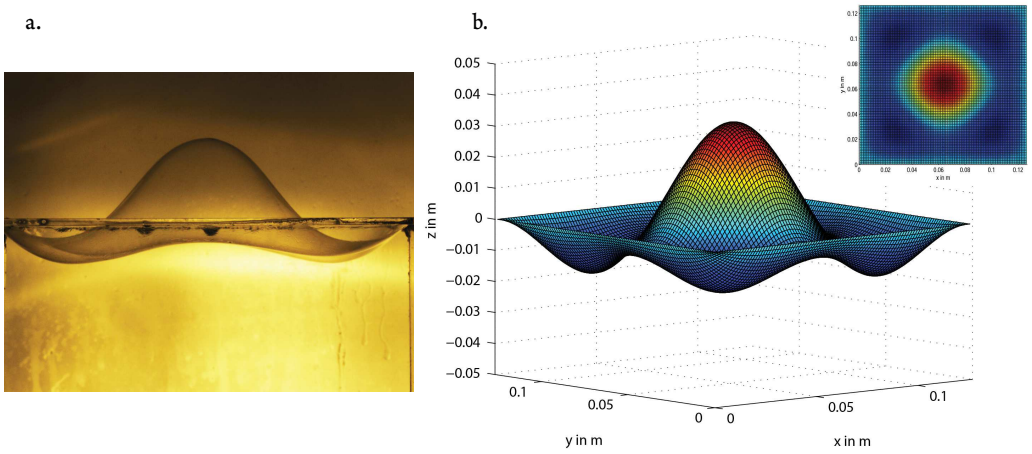

Figure 17: Visualization of mode $(3, 1) + (1, 3)$ with the numerical model, at a forcing amplitude of $A = 0.005$m (b) and the corresponding visualization in the experiment (a)

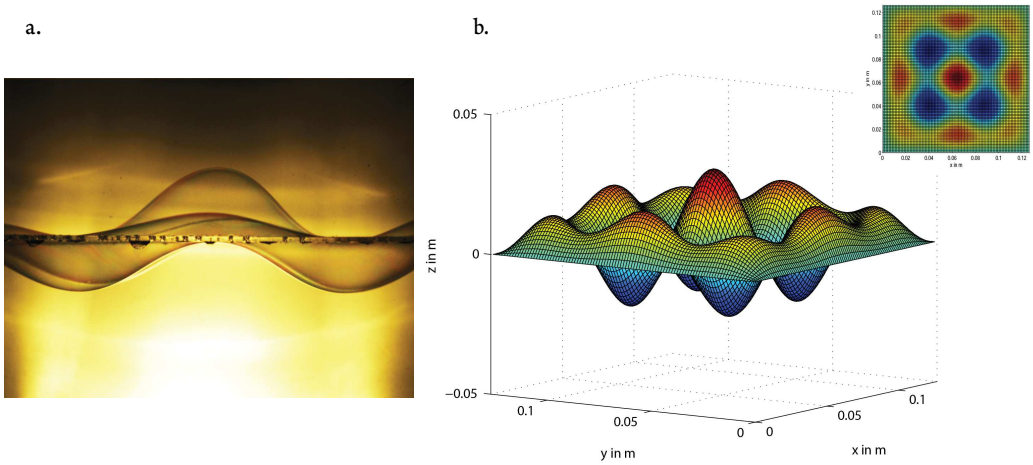

Figure 18: Visualization of mode $(5, 1) + (1, 5)$ with the numerical model, at a forcing amplitude of $A = 0.005$m (b) and the corresponding visualization in the experiment (a)

We observe that the max of amplitudes matches the pur mode that is excited in the soap film (see Fig.19). We also see that we only have odd modes as predicted by the

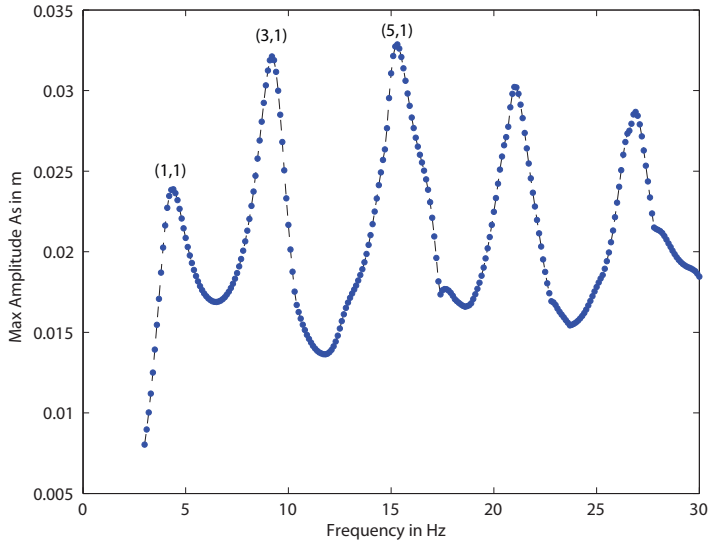

Figure 19: Maximum amplitude A_s of the soap film oscillations on the $L = 12,7$cm frame when forced in a range of frequencies

theory. Moreover the soap film response matches the experiments in terms of the shape of the film. We observe the mode (1,1) at $f = 4.13$Hz, mode (3,1)+,(1,3) at $f = 9.23$Hz and mode (5,1)+(1,5) at $f = 15,1$Hz. The mode (1,1) matches the experiments, but the rest of the modes and the max amplitude of the soap film are less in agreement with the experiments. The fact that the max amplitude is a bit lower that the one in the experiment (Fig.12) and that the modes are too close to one another is due to the fact that this model does not take into account the mass redistribution that leads to higher oscillation amplitudes and also to new mode formations. The second approximation wave velocity with added mass was tested in the numerical model to improve the results but the little changes did not improve the matching of the experimental data.

4.7 Pinch off criteria

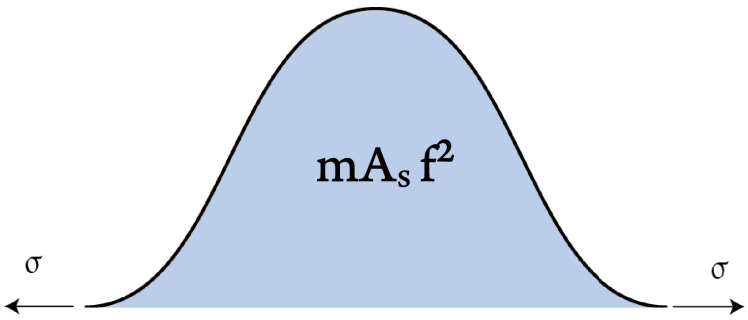

Figure 20: Schematic of the forces balance during the pinch off of a soap bubble.

Bubble pinch off arises when the destabilizing inertial driving force mA_sf^2 (with $m \sim \rho e\lambda_{nn}^2 + \rho_{air}A_s\lambda_{nn}^2$ and A_s the soap film max amplitude) exceeds the stabilizing surface tension force $2\pi\sigma\lambda_{nn}$. Thus the criteria for the critical value of the amplitude scales as:

$$A_cf^2(\rho e\lambda_{nn}^2 + \rho_{air}A_c\lambda_{nn}^2) \sim 2\pi\sigma\lambda_{nn} \tag{15}$$

We can retrieve λ_{nn} expression through the analytical solution computed in Sect.4.4:

$$\lambda_{nn} = \frac{2L}{n} \tag{16}$$

$$\omega_{nn} = \frac{c\pi n}{L}\sqrt{2} \tag{17}$$

$$n = \underset{k\in\mathbb{N}}{min}(\omega_{kk}^2 - \Omega^2) = \underset{k\in\mathbb{N}}{min}\left(\frac{2c^2\pi^2k^2}{L^2} - \Omega^2\right) \text{ and } n = 2j+1,\ j \in \mathbb{N} \tag{18}$$

$$n = \left\lfloor 2\left(\frac{\sqrt{2}}{2}\frac{\Omega L}{c\pi} - \left\lfloor\frac{\sqrt{2}}{2}\frac{\Omega L}{c\pi}\right\rfloor\right)\right\rfloor + \left\lfloor\frac{\sqrt{2}}{2}\frac{\Omega L}{c\pi}\right\rfloor \text{ and } n = 2j+1,\ j \in \mathbb{N} \tag{19}$$

By replacing λ_{nn} by its expression, the following criteria for the bubble pinch off in the soap film is then obtained:

$$A_c \sim \frac{\sqrt{8\pi\sigma f^2\rho_{air}\frac{2L}{n} + \left(f^2\rho e\frac{2L}{n}\right)^2} - f^2\rho e\frac{2L}{n}}{2f^2\rho_{air}\frac{2L}{n}} \tag{20}$$

This criteria was then plotted on the maximum amplitude regarding frequency figure, Fig.21, to verify the criteria. With a prefactor of 0.25, the criteria is consistent with the experiment.

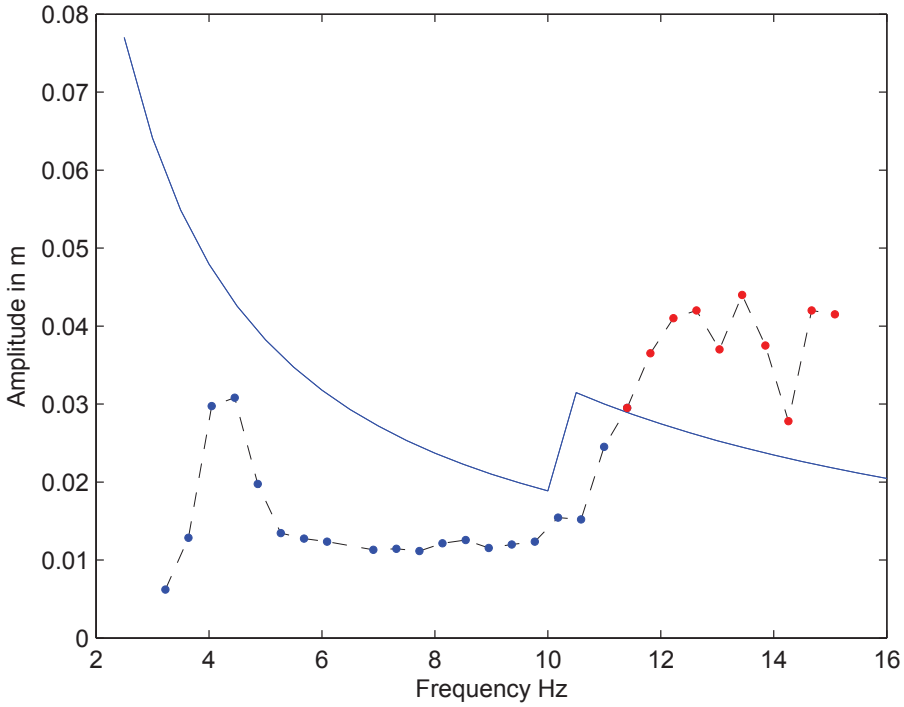

Figure 21: Maximum amplitude A_s of the soap film oscillations on the $L = 12,7$cm frame when forced in a range of frequencies in dotted lines and the criteria $A_c(f)$ in plain line.

4.8 Mass redistribution - self adaptation

The pinch off criteria and the numerical model are explaining only roughly the phenomenon. A second model [2] of the soap film taking into account the mass redistribution could more precisely describe the experiments. This model is a 1D model of a vibrating membrane with no damping and under a forcing $P\cos(2\pi ft)$ with $P = (2\pi)^2 Af^2$ (Eq.21). It also takes into account the fluid mouvement within the soap film with the inertia of the liquid balancing the marangoni forces projected along the tangential axis (Eq.22). The last equation is the mass conservation equation (Eq.23).

$$\rho e\frac{\partial^2 z}{\partial t^2} = 2\sigma\Delta z + P\cos(2\pi ft) \tag{21}$$

$$\rho e\frac{\partial u}{\partial t} = -\frac{E}{e}\frac{\partial e}{\partial x} - \rho e\frac{\partial^2 z}{\partial t^2}\frac{\partial z}{\partial x} \tag{22}$$

$$\frac{\partial e}{\partial t} + \frac{\partial (eu)}{\partial x} = 0 \tag{23}$$

In the case of a steady soap film, with have the following hypothesis:

$$z(x,t) = Z(x)\cos(2\pi ft) \tag{24}$$

$$e(x,t) = e(x) \tag{25}$$

$$u = 0 \tag{26}$$

We thus obtain after calculation (see [3] for more details) the following solutions:

$$e(x) = \frac{1}{\frac{1}{e(0)} - \frac{\rho\pi^2 f^2 Z(x)^2}{E}} \tag{27}$$

$$x = \int_0^z \frac{d\xi}{\sqrt{E\frac{\ln(e(0)^{-1} - \rho\pi^2 f^2 \xi^2) - P\xi + \beta}{2\sigma}}} \tag{28}$$

$$\int_{-\frac{L}{2}}^{\frac{L}{2}} e(x)dx = eL \tag{29}$$

This model takes into account the mass redistribution within the soap film and could be used to run a numerical model through a symbolic software, and fit more accordingly the experimental data.

4.9 Film thickness measurements

The thickness of the soap film is a crucial parameter in these experiments. It relates directly to the wave velocity in the film, the dispersion relation and the pinch off criteria. All of which are necessary to understand the dynamics of the vibrating soap film, the mode selection and the bubble ejection. Several methods used during the experiments to measure the film thickness are described below.

4.9.1 Inteference

Optical interference methods give us a good measurement of the soap film thickness variation but is proven impractical to measure the absolute thickness. A monochromatic light is pointed towards the film and by counting the fringes that appear on the surface, the difference in thickness between two points can be retrieved. However it only works when the film is very thin, otherwise the fringes are to close from one another to be accurately counted. In our case, the film had to thin by evaporation before being able to distinguish the fringes. The thickness variation between two points on the soap film is $\Delta e = \lambda N_f / 2n$ where $\lambda = 650$nm is the wave length of the monochromatic light, N_f is the number of fringes between the two considered points, $n = 1.33$ is the refractive index of the soap water. In our experiments, for the square soap film of 12.7cm under a forcing amplitude of 5mm and a frequency of 7Hz, the maximum thickness variation was $\Delta e = 4\mu\text{m} \pm 0.5\mu\text{m}$.

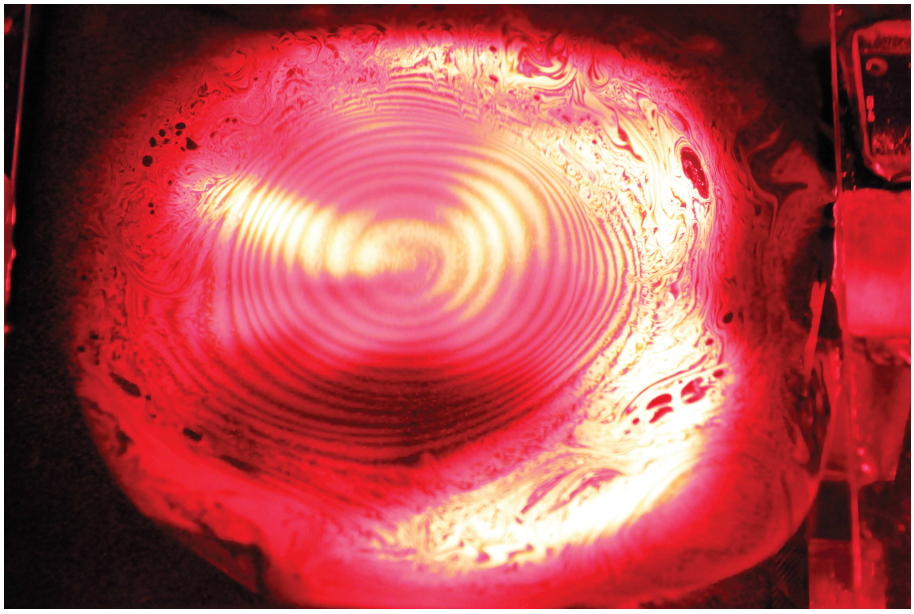

Figure 22: Inteference pattern on the vibrating soap film. In this case 15 fringes can be observed so $N_f = 15$ and that leads us to a thickness variation of $\Delta e = 3.66\mu$m between the node and the anti-node.

4.9.2 Bursting soap film

When a soap film is punctured, the speed at which a hole opens gives us an estimate of the absolute thickness of the film. Unbalanced surface tension forces at the hole edge set into motion interstitial liquid within the film, and the constant receding velocity results from mass and momentum balance ($dmv/dt = 2\sigma$). The velocity of the receding rim is constant and following $v = \sqrt{2\sigma/\rho e}$ [15,19]. Using a high speed video camera catching the reflected light on the soap film at 10 000 frames per second and a needle coated with oil to burst the film, the receding velocity can be mesured and the thickness is then derived by $e = 2\sigma/\rho v^2$. The bursting speed of the soap film is retreived from the videos (Fig.23a) by measuring the angle α in the resliced images through ImageJ (Fig.23b) . The speed is then $v = \tan(\alpha) F_r L / L_{px}$ where F_r is the framerate of the camera, L is the size of the frame in m and L_{px} is the size of the frame in pixels. The error of the measurements can be evaluated using the Klint& Mcclintock method to describe uncertainties.

$$de = \sqrt{\left(\frac{2}{\rho v^2} d\sigma\right)^2 + \left(\frac{\sigma}{\rho v^3} dv\right)^2 + \left(\frac{2\sigma}{\rho^2 v^2} d\rho\right)^2} \tag{30}$$

$$dv = \frac{F_r L}{\tan(\alpha)^2 L_{px}} d\alpha \tag{31}$$

With $\sigma = 24,3\text{mN/m} \pm 2,2\text{mN/m}$ and $\alpha = 70° \pm 1°$, the error in thickness measurements is $0,18\mu\text{m}$. The soap film created by sweeping a squeegee on the plastic frame has a steady thickness of $2\mu\text{m} \pm 0,5\mu\text{m}$ (Fig.24). The speed at which the film is created does not affect much the resulting soap film thickness. For the experiments, the soap film was created in 2 to 3s, and thus had a thickness of $2,1\mu\text{m} \pm 0,2\mu\text{m}$. The thickness of the film mainly depends on the evaporation time. The longer we wait to burst the film the thinner it becomes. A thicker film of $10\mu\text{m}$ can be obtained by pulling the frame from a soap bath.

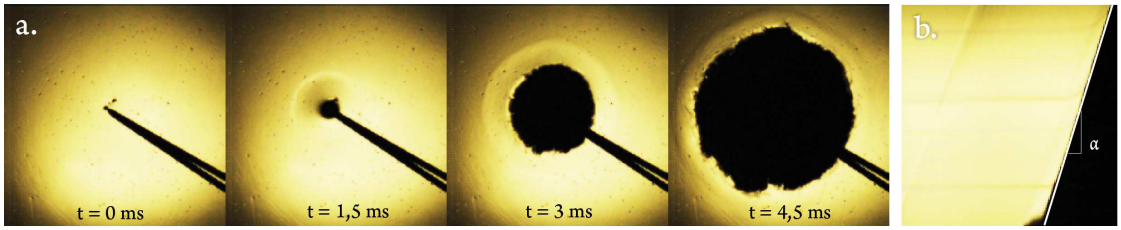

Figure 23: Bursting of soap film in a square frame. (a) Timelapse of the bursting film, (b) image processing with ImageJ to find the receding velocity

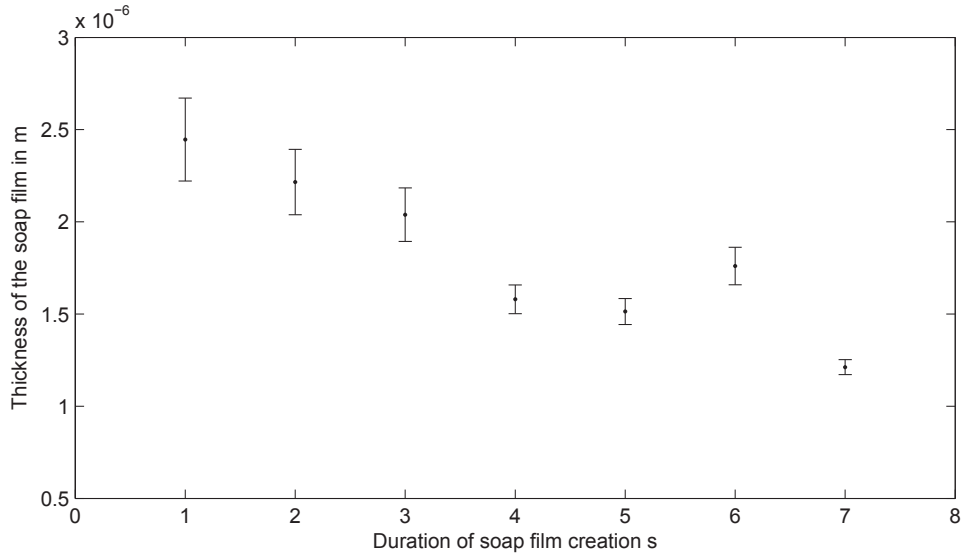

Figure 24: Soap Film Thickness

4.10 Conclustion

In this work, a range of physical phenomena observed in soap films undergoing large-amplitude oscillations in low frequency range was reported. For a clearer understanding of these mechanisms, a much more systematic investigation and a low frequency shaker (3Hz to 100Hz) that can set independantly and continuously the amplitude from 0.1 mm to 2cm are needed. This shaker coupled with a sealed humid environment could enable a more accurate and systematic study of the threshold until when the bubble pinch off arises. Also the role of several crutial parameters such as the evaporation time, the initial film thickness and surfactants needs deeper understanding.

5 A hydrodynamic analog of the casimir effect

5.1 Introduction

In quantum mechanics, the Casimir effect [6] is a mechanism by which two uncharged metallic plates in the vaccum are attracted to one another due to vaccum fluctuations.

Here we study a possible analogy of a Casimir effect in fluid mechanics. In 2009, professor Bruce C. Denardo proposed an analog of the Casimir effect [9] by studying the behavior of two partially submerged plates in a fluid. In this work we present a clearer experimental study of this hydrodynamic analog and a new model to explain the phenomenon. When the surrounding fluid is vertically excited, water waves are generated at the surface causing the plates to attract each other.

5.2 Casimir effect

There are many theories about the physics of the Casimir effect. Most of the scientific community regards this problem through zero-point energy fluctuations, that create a pressure unbalance between the two plates and the surroundings.

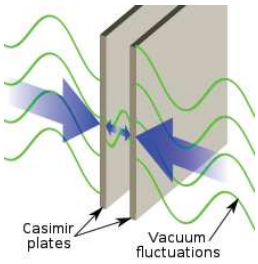

Figure 25: Illustration of the Casimir effect. Photo credit: *Emok*.

Casimir's observation was that even if the electromagnetic field is quantized, it must obey the same boundary conditions as classical electromagnetism in the presence of bulk bodies. Consequently, only some wavelengths out of the full wave spectrum would be allowed inside the two plates.

The quantization of field theory states that each point in space should have its field strength quantified, and at its most basic structure the field at each point behaves as a simple harmonic oscillator: excitations of the field correspond to elementary particles in this framework. In a harmonic oscillator, the minimum energy is not zero but $E = \hbar\omega/2$, which means that vacuum has energy. However, the existence of particles from the vacuum is limited by definition, as it has been condensed in the Heisenberg uncertainty formula: $\sigma_E \sigma_t \geqslant \hbar/2$. Thus, vacuum is restricted to the opposite side of the inequality: if an amount of energy is created in some place it is restricted by the time it can exist. Those fluctuations happen randomly, the energy of vacuum remains stable and the creation-destruction of particles occurs indefinitely.

If we have electromagnetic waves in a cavity, the energy present inside must be the energy of all the standing waves inside: $\langle E_n \rangle = \frac{1}{2}\sum_n E_n$. If we have two plates of distance d, where d is much smaller than the dimensions of the cavity, there are m modes E_m whose wavelength fits inside the plates $\left(\lambda = \frac{2d}{m}, m \in \mathbb{N}\right)$. It is clear that $m < n$, and $\langle E_m \rangle < \langle E_n \rangle$: both sums diverge but through a renormalization procedure $\delta(\langle E \rangle) = \langle E \rangle_{outside} - \langle E \rangle_{inside}$ has a real value, and $F = -\frac{\delta(\langle E \rangle)}{\delta s} \neq 0$. This is the value of the force on the surface of the plates, which can be computed as [6]:

$$F = -\frac{\hbar S c \pi^2}{240 d^4} \tag{32}$$

5.3 Experimental study

5.3.1 Background and setup

This Casimir effect analog has already been studied by Pr. Bruce Denardo from NPS [9]. In his experiment, he parametrically excites random Faraday waves at the surface of a container. A spectrum of 10 to 20 Hz is used, and they get a subharmonic response between 5 to 10 Hz, for which some wavelengths fit inside the container and others do not, thus generating a sort of Casimir analog. Although the results seem to be coherent, the model explaining his experimental results seems flawed. He considers travelling waves whereas we only noticed standing waves in the experiment. Moreover, he does not consider the wetting of the plates that appears to be very important in our case.

In our study we focused on a simplier problem than what was previously done [9]. We considered two square plates of length a partially submerged in a bath of water vertically excited by a shaker (Fig.26). The plates are suspended by wires of lenght L so as to act as a linear pendulum and seperated by a distance d. As opposed to the experiment by Pr. Bruce Denardo, we only excited one stationary wave of wavelength λ, measured the attractive force acting on the plates through their displacement and recorded the amplitude A of the surface waves thanks to a high speed video camera (Fig.27). We assumed the displacement to be horizontal and that all the forces are applied at the same point since $d << L$ and $a << L$. We neglected the attractive force due to the suface tension between the plates since $d >> \kappa^{-1} = \sqrt{\frac{\sigma}{\rho g}} \sim 2$mm Through an equilibrium analysis of the forces at work (gravity, string tension and the *attratcive force*) in the linear case of small displacements, we can deduce the following relation between the horizontal displacement x and the *attractive force* applied on a plate F :

$$F = m^* g \frac{x}{L} \text{ , with } m^* \text{ the mass of the plate considering the buoancy forces} \tag{33}$$

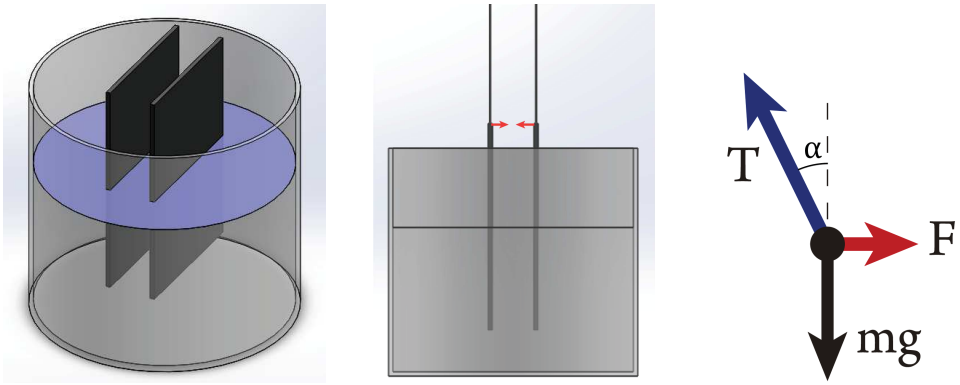

(a) (b) (c)

Figure 26: (a)&(b) Schematics of the experimental setup. (c) Force equilibrium on the plates (T for the tension, mg for gravity and F for the *attractive force*).

We shall operate in a framework where linear wave theory calculations are possible. We shall also assume small perturbations in the surface in order to consider the water-wave dispersion relation [10]:

$$(2\pi f)^2 = \left(g\frac{2\pi}{\lambda} + \frac{\sigma}{\rho}\left(\frac{2\pi}{\lambda}\right)^3 \right) \tanh(\frac{2\pi h}{\lambda}) \tag{34}$$

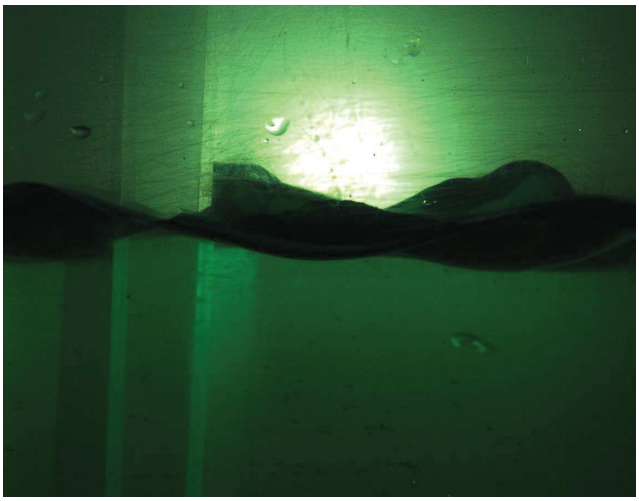

Figure 27: Example of video footage taken with a high-speed video camera

We worked in the $9 - 14$Hz range of frequencies, which allows us to select waves that fit between the plates and others that do not in a relatively reduced spectrum. This reduces instrumental errors related to the harmonic distortion of the loudspeaker used for driving the system.

5.3.2 Experimental results

The first series of experiments were conducted at a driving frequency of $12\,Hz$, which created a subharmonic response in the form of Faraday waves at the surface with a frequency of 6Hz. The response of the surface waves is not linear. At low amplitude, small radial waves appear on the surface (Fig.28.a). At higher amplitude, Faraday cross-waves with high amplitude appear on the surface in lattices such as hexagons (Fig.28.b) By driving the bath higher, the waves move to the boundaries and nearly no waves stands in the center (Fig.28.c) If we drive the bath even more, the interface breaks and the system becomes chaotic. In our experiments, we remained in the second regime with cross-waves. In that case, the wavelength calculated with the dispersion relation is $\lambda = 4.8$cm.

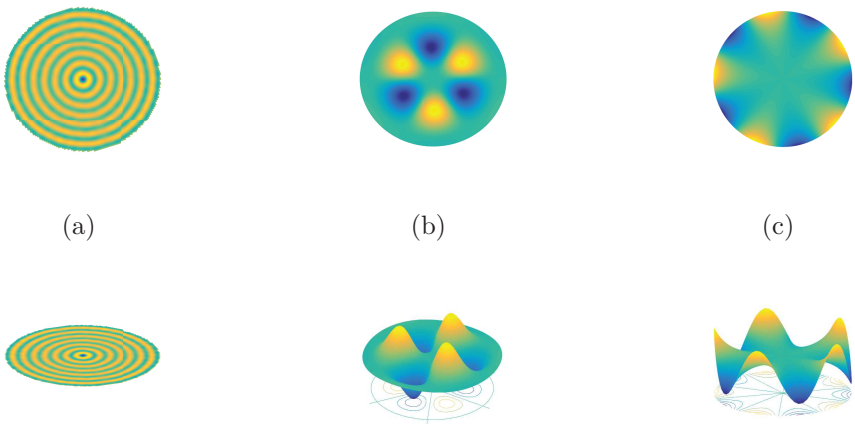

(a) (b) (c)

(d) (e) (f)

Figure 28: (a) and (d): Radial waves. (b) and (e): Cross waves on the surface. (c) and (f): Edge waves.

We performed a series of experiments for $d = 1, 2, 3$cm. We found a linear correlation between the intensity of the waves ($\propto A^2$, here defined as $A^2_{rms} = \frac{A^2}{2}$ for sinusoidal waves) and the force exerted on the plates ($\propto x$, where x is the displacement from the equilibrium position Eq.33) for the cases in which $d \lesssim \frac{\lambda}{2}$. Fig.29 shows the best fitting line along with the results obtained. The equation gives

$$\frac{F}{g} = 8.2\, A^2_{rms} - 8.0 \tag{35}$$

where the term in the left states for *equivalent mass* following Eq.33, given in milligrams, and the *RMS Amplitude* is given in millimeters. This result will be compared later on through our simple theorical model.

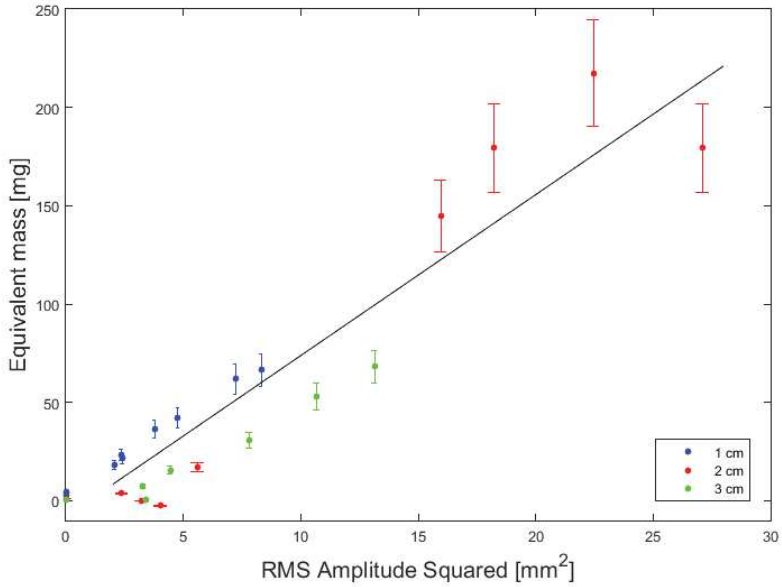

Figure 29: Results at different values of separation d and best fitting line.

Bigger separation to wavelength ratios were also studied but no significant displacement was observed suggesting that when the surface waves are able to fit inside the plates the hydrodynamical effects happening are greatly reduced.

5.4 Theorical model

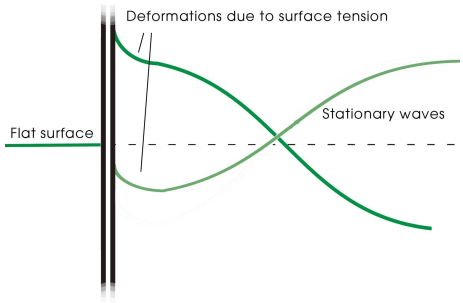

Figure 30: Approximations used in our model

The experiment shows that there is an asymmetry at the boundaries leading to a pressure unbalance. Outside the plates, the mean fluid height of the fluid-plate contact

is higher than inside the plates (Fig.30). At the maximum of the oscillations the fluid seems to reach a height close to that of the other peaks in the fluid $z = A$. However, the minimum is much higher than the minimum of the surrounding waves. In fact, given the observed deformations of the interface, it could be stated that the interface stays near $z = 0$ during the minimum. This effect, due to the meniscus, changes the wave field near the plates, so as it seems centered in $z = \frac{A}{2}$ rather than $z = 0$. The interface can thus be considered as :

$$\zeta = \frac{A}{2}\left(1 + \cos(\Omega t)\right) cos(ky), \quad \text{given that we place ourselves in a maximum,} \quad x = \frac{2\pi}{k} \tag{36}$$

The hydrostatic pressure difference applied on the plates can be computed this way:

$$p(y,t) = \rho g \zeta(y,t) \tag{37}$$

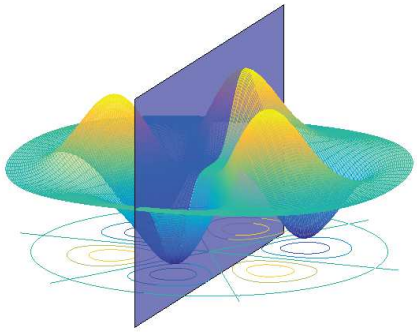

Figure 31: Position of the plates relative to the waves for the case of 12 Hz.

In the case of 12 Hz, for which a significant amount of data has been registered, the waves recorded are mainly in the form of *Cross waves* as defined in Fig.28 and it is possible to observe that the plates are always positioned in the antinodes of the waves present. Thus, as illustrated in Fig.31 the integral in the y direction (represented by the plane in blue) would be correctly approximated to a half wavelengths. The resultant mean force is

$$F = \left\langle \int p \, dS \right\rangle_T \tag{38}$$

$$F = \left\langle \int_0^{\lambda/2} \rho g \zeta^2 \, dy \right\rangle_T = \frac{3}{32} \rho g A^2 \lambda \tag{39}$$

$$\frac{F}{g} = \frac{3}{16} \rho \lambda \, A_{rms}^2, \text{ where } \frac{3}{16} \rho \lambda \approx 9.1 \tag{40}$$

This model is thus a relevant first order approximation of the experimental results obtained for the case of 12 Hz where we had :

$$\frac{F}{g} = 8.2 \, A_{rms}^2 - 8.0 \tag{41}$$

5.5 Conclusion

In this work, we observed a similar phenomenon as reported by Pr. Bruce Denardo [9]. Two plates partially submerged in a vertically excited bath of water undergo a attractive force. This phenomenon was exhibited when the wavelength of the forced surface wave is larger than twice the distant between the plates. Moreover this *attractive force* seems to follow this scale law : $F \sim \rho g \lambda A^2$. For a clearer understanding of these mechanisms, a better understanding of the effort excerted by a fluid on a movable boundary must be studied and a more precise experimental setup must be considered. This setup should include the following features: a bigger bath such that the boundary effects are diminished, a better shaking system, use longer wires and heavier plates to maintain the wires in tension to be closer to the linear pendulum hypethesis, add more depth in the bath to be in better accordance to the deep water wave approximation and use a fluid that is not as much affected by surfactants as water is. A more interesting case should also be studied. Knowing that the meniscus of the fluid-plate contact is responsible for the asymmetry leading to the hydrostatique overpressure pushing the plates together, using hydrophobic plates that lead to an inverted meniscus could generate a hydrostatic underpressure force, acting as a repulsive force between the two plates.

References

[1] VO Afenchenko, AB Ezersky, SV Kiyashko, MI Rabinovich, and PD Weidman. The generation of two-dimensional vortices by transverse oscillation of a soap film. *Physics of Fluids (1994-present)*, 10(2):390–399, 1998.

[2] A Boudaoud, Y Couder, and MB Amar. Self-adaptation in vibrating soap films. *Physical review letters*, 82(19):3847, 1999.

[3] Arezki Boudaoud. Membranes élastiques et capillaires: instabilités, singularités et auto-adaptation, 2001.

[4] H Brenner. *Interfacial transport processes and rheology*. Elsevier, 2013.

[5] John W.M. Bush. Pilot-wave hydrodynamics. *Annual Review of Fluid Mechanics*, 47:269–292, 2015.

[6] Hendrick BG Casimir. On the attraction between two perfectly conducting plates. 51(793):150, 1948.

[7] Y Couder, JM Chomaz, and M Rabaud. On the hydrodynamics of soap films. *Physica D: Nonlinear Phenomena*, 37(1):384–405, 1989.

[8] Yves Couder, Suzie Protiere, Emmanuel Fort, and Arezki Boudaoud. Dynamical phenomena: Walking and orbiting droplets. *Nature*, 437(7056):208–208, 2005.

[9] Bruce C Denardo, Joshua J Puda, and Andres Larraza. A water wave analog of the casimir effect. *American Journal of Physics*, 77(12):1095–1101, 2009.

[10] V Dj Djordjevic and Larry G Redekopp. On two-dimensional packets of capillary-gravity waves. *Journal of Fluid Mechanics*, 79(04):703–714, 1977.

[11] W Drenckhan, B Dollet, S Hutzler, and F Elias. Soap films under large-amplitude oscillations. *Philosophical Magazine Letters*, 88(9-10):669–677, 2008.

[12] A Eddi, A Decelle, E Fort, and Y Couder. Archimedean lattices in the bound states of wave interacting particles. *EPL (Europhysics Letters)*, 87(5):56002, 2009.

[13] Michael Faraday. On the forms and states assumed by fluids in contact with vibrating elastic surfaces. *Philos. Trans. R. Soc. London*, 121(319):1831, 1831.

[14] Daniel M Harris and John WM Bush. Generating uniaxial vibration with an electrodynamic shaker and external air bearing. *Journal of Sound and Vibration*, 334:255–269, 2015.

[15] WR McEntee and KJ Mysels. Bursting of soap films. 1. an experimental study. *The Journal of Physical Chemistry*, 73(9):3018–3028, 1969.

[16] H Minami. Added mass of a membrane vibrating at finite amplitude. *Journal of Fluids and Structures*, 12(7):919–932, 1998.

[17] S Protiere, S Bohn, and Y Couder. Exotic orbits of two interacting wave sources. *Physical Review E*, 78(3):036204, 2008.

[18] G. Pucci, D. M. Harris, and J. W. M. Bush. Partial coalescence of soap bubbles. *Physics of Fluids*, 27(6), 2015.

[19] D Quéré, F Brochard-Wyart, and PG de Gennes. *Gouttes, Bulles, Perles et Ondes*. Belin, 2002.

[20] Singiresu S Rao. *Vibration of continuous systems*. John Wiley & Sons, 2007.

[21] Karim Shariff and Anthony Leonard. Vortex rings. *Annual Review of Fluid Mechanics*, 24(1):235–279, 1992.

[22] D Terwagne and JWM Bush. Tibetan singing bowls. *Nonlinearity*, 24(8):R51, 2011.

[23] Jose M Vega, FJ Higuera, and PD Weidman. Quasi-steady vortical structures in vertically vibrating soap films. *Journal of Fluid Mechanics*, 372:213–230, 1998.

[24] Øistein Wind-Willassen, Jan Moláček, Daniel M Harris, and John WM Bush. Exotic states of bouncing and walking droplets. *Physics of Fluids (1994-present)*, 25(8):082002, 2013.

A Bouncing Droplet Demonstration

Design by Julio Quintela Casal & Victor Prost

We here present the design of a low-cost bouncing-droplet demonstration device suitable for exploratory and educational purposes. It consists of seven main components: a loudspeaker, an audio amplifier, an LED strip, two petri dishes, Silicon oil and a signal generator in the form of a smartphone or computer.

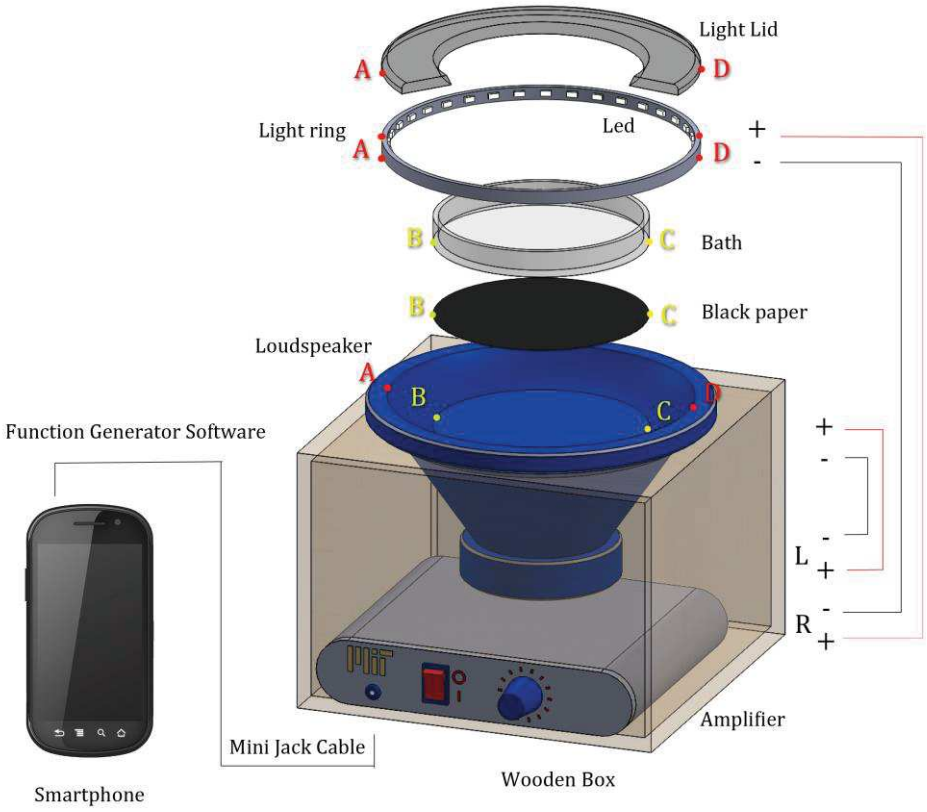

Assembled system

Assembly Procedure

1. *Vibrating Bath* - Paste a black sheet of paper to the base of the small petri dish in order to optimize visualization. Glue the petri dish to the cone of the loudspeaker, being sure to level the system. (Connect B and C)
2. *Light ring* – Cut off the base of the 6.5" Petri dish and glue the LED strip to the remaining plastic ring's inner surface. Add an optional light lid (made out of cardboard) to optimize visualization. (Connect A and D)
3. *Power* - Using DC wires, connect the two electrical pins of the loudspeaker to the Left channel of the amplifier. Connect the two pins of the LED strip to the Right channel of the amplifier.
4. *Fill the bath* – Pour Silicon oil into the inner Petri dish, creating a fluid layer of approximately 3mm depth. *Optional:* a substitute for silicon oil is *Linseed oil*, a vegetable oil used as varnish and easy to find in stores.
5. *Signal generator* - Connect the smartphone or computer with the mini-Jack cable. Start and configure the Function Generator App. Click on OUT so the system starts emitting, and adjust the smartphone volume to the maximum. Configure Channel 1 to Left and Channel 2 to Right. The configuration parameters are:

Channel	Left	Right
Wave type	Sine	Square
Frequency for 20 cSt Silicon oil /Linseed oil	80 Hz / 60 Hz	40 Hz / 30 Hz
Duty	-	20%
Amplitude	15%	100%

   Turn on the amplifier and slowly increase the Bass up to 75% of the maximum. Turn the Volume on. The system should start making a low noise. By increasing the Volume, vibration should appear. Faraday waves should arise at high volume. The system is now ready to operate.
6. *Mounting (Optional)* – Affix amplifier and loudspeaker in a box.

Some experiments

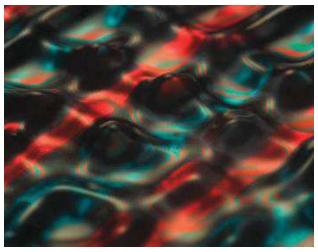

1. *Faraday waves:*
   Play with the Volume and the Bass in order to find the Faraday threshold, above which waves are excited.

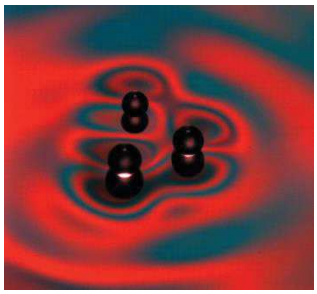

2. *Bouncing droplets:*
   a. Increase the Volume and the Bass but stay well below the Faraday threshold. (The surface of the water should remain planar in the absence of drops).
   b. Use a toothpick or needle to create drops by dipping it into the bath and extracting it swiftly.
   c. You can also create several droplets and observe their interactions.
   d. The drop should appear stationary if you synchronize the LED lights and the loudspeaker. Altering the phase of the LED lights will change the apparent height of the drop. To see the bouncing, detune the LED lights to 41Hz.

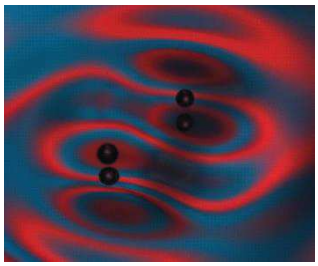

3. *The walking droplet:*
   a. Create a small bouncing droplet (~1mm diameter).
   b. Increase the Volume and the Bass until the droplet starts to walk. If you cross the Faraday threshold prior to the onset of walking, try a smaller drop.
   c. Create multiple walkers to observe bound states: orbitals, ratcheting pairs, the promenade mode, etc…

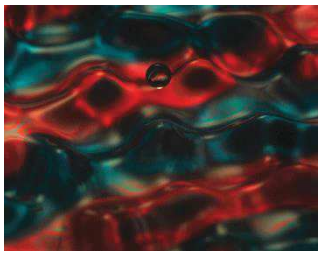

4. *Breaking the interface:*
   Increase the Volume and the Bass in order to cross the Faraday threshold. Continue increasing the Volume and the Bass until the interface breaks, creating a multitude of droplets.

Purchasing Details

Loudspeaker ($21.78) is a commercially available woofer (6.5" diameter, 50 watts, 8Ω impedance, available at Dayton Audio DC160-8)
http://www.parts-express.com/dayton-audio-dc160-8-6-1-2-classic-woofer--295-305

Male to Male 3.5mm mini-Jack Cable ($1.59)
http://www.amazon.com/niceeshop-3-5mm-Stereo-Audio-Cable/dp/B00HIDEE22/ref=sr_1_26?s=audio-video-accessories&ie=UTF8&qid=1430855605&sr=1-26

Amplifier ($13.95) is a radio booster MP3 stereo (200W max power output at 2Ω impedance - 50W@8Ω -, available at TMS 200W)
http://www.amazon.com/Hi-Fi-Amplifier-Booster-Stereo-Motorcycle/dp/B00M0XSJX0

Amplifier power supply cable ($7.48)
http://www.amazon.com/Replacement-Adapter-Charger-Benq-Monitors/dp/B003Z6ZR5O

LED strips ($13.25) are 5050 SMD LED lights (6600 Lumen, dimmable LED available at NFLS)
http://ledlightscompare.com/led-light-strips-led-tape-light-with-18-smdsft-3-chip-smd-led-5050-p-544.html

4" (or 10cm) diameter petri dish ($0.5) to contain the oil bath
http://www.amazon.com/SEOH-Petri-Dishes-20-pk/dp/B0007656QA

6.5"diameter petri dish ($1) to be used as a frame for the LED lights
http://www.amazon.com/Karter-Scientific-Plastic-150x15mm-Sterile/dp/B005Z4QV4U

2 Channel function generator App /Software (Free)
https://play.google.com/store/apps/details?id=com.keuwl.functiongenerator

Smartphone/ Computer to be used as a 2 channel function generator using the above app to drive the loudspeaker through the amplifier.

Silicon oil (20ctS)
http://www.sigmaaldrich.com/catalog/product/aldrich/378348?lang=en&region=US

Linseed oil
http://www.amazon.com/SUNNYSIDE-CORPORATION-87232-1-Quart-Linseed/dp/B000C016PG/

DC wires for applications in electronics

Glue (e.g. McMaster Acrylics glue).

Black paper.

Total Cost: $60